

iFCTN: Folding-Free Fully-Connected Tensor Network Decomposition for Tensor Completion

Ziyi Gan¹ Chunfeng Cui^{1*}

¹ Beihang University, Beijing, China

ganziyi@buaa.edu.cn, chunfengcui@buaa.edu.cn

Abstract

The fully-connected tensor network (FCTN) decomposition has recently exhibited strong modeling capabilities by connecting every pair of tensor factors, thereby capturing rich cross-mode correlations and maintaining invariance under mode transpositions. However, this advantage comes with an inherent limitation: updating the factors typically requires reconstructing auxiliary sub-networks, which entails extensive and cumbersome (un)folding. In this study, we propose intra-block FCTN (iFCTN) decomposition, a novel (un)folding-free variant of FCTN decomposition that streamlines computation. We parameterize each FCTN factor through Khatri-Rao products, which significantly reduces the complexity of reconstructing intermediate sub-networks and yields subproblems with well-structured co-efficient matrices. Furthermore, we deploy the proposed iFCTN decomposition on the representative task of tensor completion and design an efficient proximal alternating minimization algorithm while retaining convergence guarantees. Extensive experiments demonstrate that iFCTN outperforms or matches state-of-the-art methods with comparable computational cost.

1. Introduction

With rapid advances in science and technology, high-dimensional datasets (e.g., multispectral images and traffic-flow measurements) have become pervasive in practice and are naturally represented as tensors. A tensor extends the concept of a matrix to higher orders, with entries indexed by multiple (continuous or discrete) variables. Tensor decompositions are powerful tools for modeling and processing such high-order data, and their applications are ubiquitous in machine learning [1, 17, 21], signal processing [4, 5], and much more. Conceptually akin to matrix factorization, tensor decomposition is the art of disassembling a multi-dimensional array into smaller factors [2]. Over the past decades, several prominent models have been es-

tablished, including Tucker decomposition [7, 19], CAN-DECOMP/PARAFAC (CP) decomposition [11], and tensor singular value decomposition (t-SVD) [10].

In recent years, numerous tensor network (TN) decompositions have been widely adopted in computational mathematics and numerical analysis, exhibiting superior properties such as extreme compression and efficient computation [3, 9]. Among them, the tensor-train (TT) decomposition [16] stands out as a seminal milestone. TT factors an N th-order tensor into a sequence of multilinear products over a set of cores. Specifically, the first and last cores are matrices, while the remaining $N - 2$ intermediate cores are third-order tensors, as illustrated in Fig. 1. Subsequently, the tensor ring (TR) decomposition [26] extends TT by replacing the boundary matrices with third-order cores and closing the chain via an additional circular contraction.

Introduced in 2021, the fully connected tensor network (FCTN) decomposition [29] represents a significant advancement over TT and TR. Unlike its predecessors, which only establish connections between adjacent factors, FCTN decomposes an N -th order tensor into N core tensors, establishing a connection between *every* pair of factors. This fully-connected topology grants FCTN the superior capability to characterize the intrinsic correlations between any two modes of the tensor, making it highly effective for tensor completion (TC) [8, 13, 20, 24]. Subsequently, several variants of FCTN were also proposed, including SVDins-FCTN [30], N-FCTN [6], revealFCTN [14], T-FCTN [15], NL-FCTN, and nonlocal patch-based FCTN [27].

Although FCTN has recently been shown to capture rich cross-mode correlations and to preserve invariance under mode transposition, the full connectivity and the high-order nature of its core tensors inherently introduce **higher computational complexity** and potential **parameter redundancy** [28]. Specifically, updating FCTN factors typically requires reconstructing auxiliary sub-networks and repeatedly (un)folding intermediate tensors. Specifically, for an N th-order tensor, updating any single factor necessitates forming a dedicated sub-network from the remaining $N - 1$ factors. Consequently, an N -way tensor entails

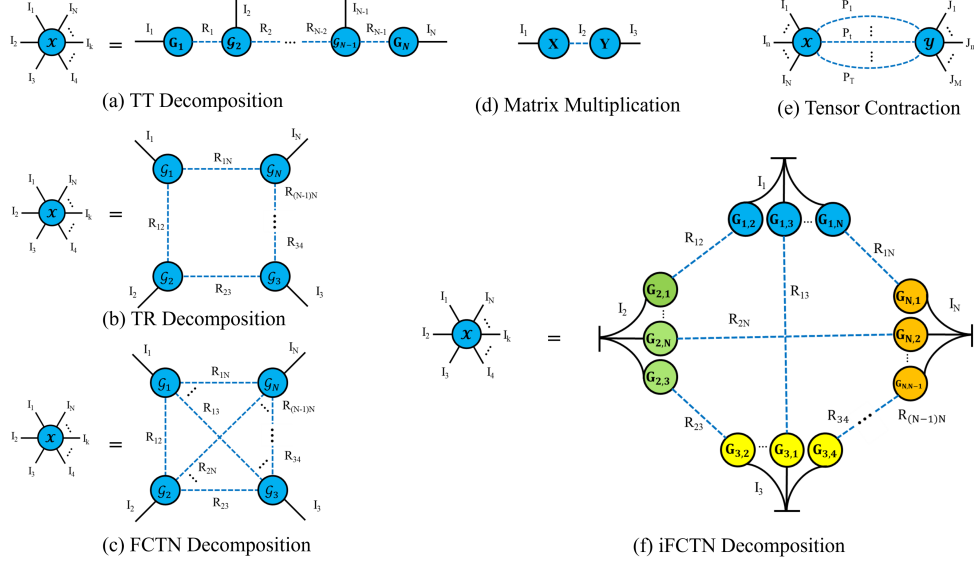


Figure 1. A graphical representation of TT, TR, FCTN and the proposed iFCTN decompositions. Here, the **blue dotted lines** denote matrix multiplications or tensor contractions, and the KR product is visually depicted as the “cherry stem”. In contrast to the TT, TR, and FCTN, which employ tensor factors, iFCTN represents each tensor factor as a “cherry chain”, whose components (“cherries”) are matrices.

N such constructions per iteration, and these sub-networks must be rebuilt after every update. This reconstruction, with high computational cost and substantial memory overhead, slows practical training—particularly for large-scale, high-order tensors common in computer vision. Addressing this computational burden while preserving FCTN’s expressive power is a critical area of research [18].

To address these challenges, we revisit FCTN from an intra-block perspective and parameterize each tensor factor via Khatri–Rao (KR) products. This simple yet pivotal design preserves cross-mode expressivity while rendering the underlying linear algebra unfolding-free and amenable to efficient solvers. The main **contributions** of this paper are summarized as follows:

- We first propose a novel intra-block FCTN (iFCTN) framework, an (un)folding-free variant of FCTN that relies solely on matrix factors while capturing rich cross-mode correlations among the tensor factors (Section 3). By decomposing the tensor factors into matrix factors (i.e., cherry tensor and cherry products) via the KR product, iFCTN admits an explicit expression for the sub-network (i.e. cherry sub-network).
- We then apply iFCTN to the TC problem (iFCTN-TC), directly leveraging the cherry-based parameterization for scalable optimization (Section 4). Our complexity analysis reveals that iFCTN effectively reduces both storage and computational complexities. Moreover, we establish convergence guarantees for the proposed proximal alternating minimization (PAM) solver.
- We assess the performance of iFCTN-TC on five bench-

mark datasets under eight random and fiber-wise missing scenarios, and it consistently attains superior accuracy with comparable computational cost, thereby validating its effectiveness and robustness (Section 5).

2. Notations and Preliminaries

In this paper, we denote vectors, matrices and tensors as \mathbf{x} , \mathbf{X} , \mathcal{X} , respectively. Given an N th-order tensor $\mathcal{X} \in \mathbb{R}^{I_1 \times I_2 \times \dots \times I_N}$, its mode- n unfolding is $\mathcal{X}_{(n)} \in \mathbb{R}^{I_n \times \prod_{k=1, k \neq n}^N I_k}$. Here, $n \in [N]$ and $[N] = \{1, \dots, N\}$. Given two matrices $\mathbf{A} \in \mathbb{R}^{m \times r}$ and $\mathbf{B} \in \mathbb{R}^{n \times r}$, their Khatri-Rao product is $\mathbf{C} = \mathbf{A} \odot \mathbf{B} \in \mathbb{R}^{mn \times r}$, where $c_{(i-1)n+j, l} = a_{il}b_{jl}$ for any $i \in [m]$, $j \in [n]$, and $l \in [r]$.

Definition 1 (FCTN Decomposition [29]). *FCTN decomposes $\mathcal{X} \in \mathbb{R}^{I_1 \times I_2 \times \dots \times I_N}$ into N tensor factors*

$$\begin{aligned} & \mathcal{X}(i_1, i_2, \dots, i_N) \\ &= \sum_{r_{1,2}=1}^{R_{1,2}} \sum_{r_{1,3}=1}^{R_{1,3}} \dots \sum_{r_{1,N}=1}^{R_{1,N}} \sum_{r_{2,3}=1}^{R_{2,3}} \dots \sum_{r_{2,N}=1}^{R_{2,N}} \dots \sum_{r_{N-1,N}=1}^{R_{N-1,N}} \\ & \{ \mathcal{G}_1(i_1, r_{1,2}, r_{1,3}, \dots, r_{1,N}) \\ & \quad \mathcal{G}_2(r_{1,2}, i_2, r_{2,3}, \dots, r_{2,N}) \dots \\ & \quad \mathcal{G}_k(r_{1,k}, r_{2,k}, \dots, r_{k-1,k}, i_k, r_{k,k+1}, \dots, r_{k,N}) \dots \\ & \quad \mathcal{G}_N(r_{1,N}, r_{2,N}, \dots, r_{N-1,N}, i_N) \}. \end{aligned} \quad (1)$$

Here, $\mathcal{G}_k \in \mathbb{R}^{R_{1,k} \times \dots \times R_{k-1,k} \times I_k \times R_{k,k+1} \times \dots \times R_{k,N}}$ denotes a factor tensor. There are N factors in total.

Recently, FCTN and its variants [20, 28] demonstrate high efficiency and stability in many applications. However,

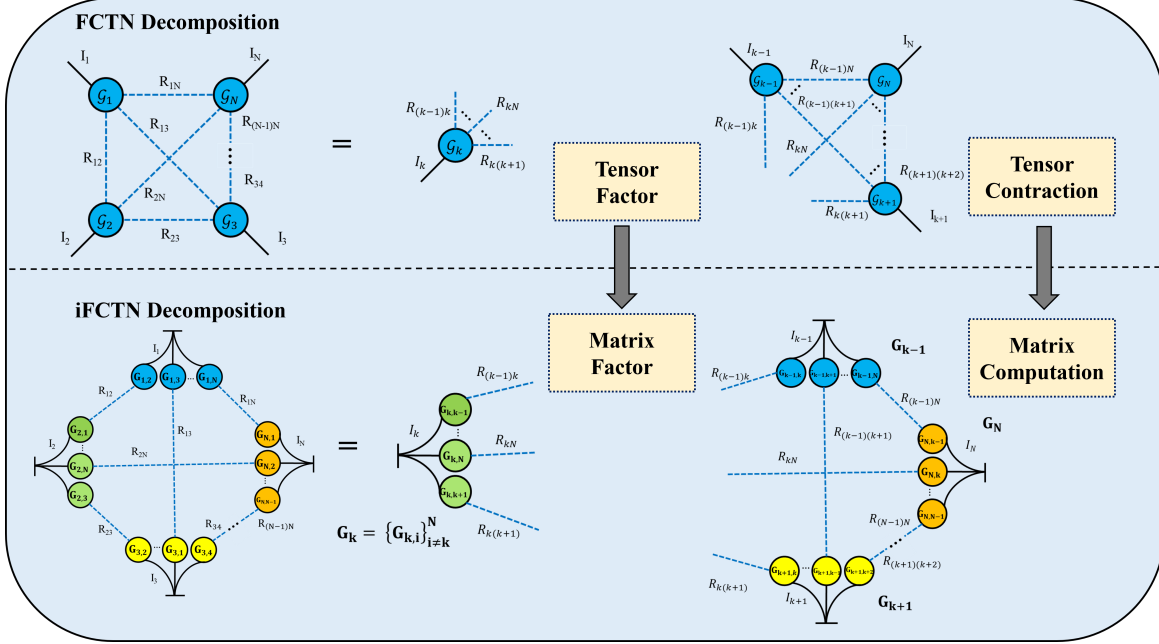


Figure 2. A comparative analysis of sub-network: FCTN versus the proposed iFCTN Decomposition.

computing the FCTN decomposition, as in (1), demands either numerous summation loops or extensive large-scale tensor folding/unfolding to leverage matrix operations. To address these limitations, this paper introduces a relaxation technique based on the KR product.

3. iFCTN Decomposition

Our proposed iFCTN is derived from FCTN, as depicted in Fig. 1 (d). The pivotal alteration lies in parameterizing each tensor factor as a sequence of matrices, thereby achieving a matrix-based realization of FCTN. This reformulation enables all updates to be performed via matrix computations without tensor contractions. Furthermore, by leveraging the KR product, we establish several structural results that underpin the proposed iFCTN.

We begin with the following definition, which decomposes a tensor into small matrices factors.

Definition 2 (Mode- k Cheery Tensor). A tensor $\mathcal{G} \in \mathbb{R}^{R_{1:k-1} \times I_k \times R_{k+1:N}}$ is referred to as a mode- k KR-product tensor, or simply a mode- k cheery tensor, if its k -th mode unfolding admits a KR factorization as follows,

$$(\mathcal{G}_{(k)})^\top = \mathbf{M}_N \odot \cdots \odot \mathbf{M}_{k+1} \odot \mathbf{M}_{k-1} \cdots \odot \mathbf{M}_1, \quad (2)$$

where $\mathbf{M}_i \in \mathbb{R}^{R_i \times I_k}$ are cheery factors of \mathcal{G} . For convenience, we also denote

$$\mathcal{G} = \mathcal{CT}_k \left(\{M_i\}_{i=1, i \neq k}^N \right).$$

We term \mathcal{G} in (2) a cheery tensor, as its structure, depicted in Fig. 1, visually resembles “a string of cherries” hanging from their “stems”: the KR product forms the “stems” that connect the smaller matrices (“cherries”). This representation simultaneously preserves an explicit dependence on the underlying tensor structure.

In fact, when $m \in [I_k]$, (2) reduces to¹:

$$(\mathcal{G}_{(k)}(:, m))^\top = \mathbf{M}_N(:, m) \odot \cdots \odot \mathbf{M}_{k+1}(:, m) \odot \mathbf{M}_{k-1}(:, m) \cdots \odot \mathbf{M}_1(:, m).$$

This is precisely the rank-one decomposition of $\mathcal{G}(:, \dots, m, \dots, :)$. Hence, every layer of the cheery tensor along the k -th mode is itself a rank-one tensor. Indeed, Definition 2 is inspired by the CP decomposition and forms the cornerstone of our iFCTN decomposition.

In practice, there is no need to compute the cheery tensor (2). Instead, all storage and computations are performed directly on the cheery factors $\{\mathbf{G}_{k,i}\}$. For brevity, we hereafter denote the set of cheery factors at the k -th mode (“ k -th string of cherries”)² by

$$\mathbf{G}_k = \{\mathbf{G}_{k,i}\}_{i \neq k}^N, \quad \mathbf{G}_{k,i} \in \mathbb{R}^{R_{k,i} \times I_k}. \quad (3)$$

With Definition 2, folding/unfolding is no longer required: tensor products are expressed directly in the matrix form, which streamlines the construction of the tensor network.

Next, we present how to connect two cheery tensors.

¹The notations $A(m, :)$ and $A(:, m)$, adopted from MATLAB, denote the m -th row and m -th column of matrix A , respectively.

Definition 3 (Cherry Product). Consider two cherry tensors $\mathcal{A} = \mathcal{CT}_k(\{\mathbf{A}_i\}_{i \neq k}) \in \mathbb{R}^{P_1:k-1 \times I_k \times P_{k+1}:N}$ and $\mathcal{B} = \mathcal{CT}_t(\{\mathbf{B}_i\}_{i \neq k}) \in \mathbb{R}^{Q_1:t-1 \times J_t \times Q_{t+1}:M}$. Let $\alpha \in [N]$, $\beta \in [M]$, $\mathbf{n} = [N] \setminus \alpha$, and $\mathbf{m} = [M] \setminus \beta$. Suppose that $P_\alpha = Q_\beta$. Then their cherry product yields an $(N+M-2)$ th order tensor as follows,

$$\mathcal{C}(i_{n_1}, \dots, i_{n_{N-1}}, j_{m_1}, \dots, j_{m_{M-1}}) = \prod_{n_i} \mathbf{A}_{n_i}(i_{n_i}, i_{n_{\bar{k}}}) \prod_{m_j} \mathbf{B}_{m_j}(j_{m_j}, j_{m_{\bar{t}}}) (\mathbf{A}_\alpha^\top \mathbf{B}_\beta)_{i_{n_{\bar{k}}}, j_{m_{\bar{t}}}}. \quad (4)$$

Here, $\bar{k} = k$ if $\alpha > k$ and $k-1$ otherwise; similarly, $\bar{t} = t$ if $\beta > t$ and $t-1$ otherwise.

Remark 1. For simplicity, let $M = N = 3$, and consider a mode-2 cherry tensor $\mathcal{A} \in \mathbb{R}^{P \times I \times R}$ and a mode-3 cherry tensor $\mathcal{B} \in \mathbb{R}^{Q \times R \times J}$. Then their Cherry product yields a tensor of size $\mathbb{R}^{P \times I \times Q \times J}$ written as follows,

$$\mathcal{C}(i, j, k, l) = \mathbf{A}_1(i, j) \mathbf{B}_1(k, l) (\mathbf{A}_3^\top \mathbf{B}_2)_{j, l},$$

where $\mathbf{A}_1 \in \mathbb{R}^{P \times I}$, $\mathbf{A}_3 \in \mathbb{R}^{R \times I}$, $\mathbf{B}_1 \in \mathbb{R}^{Q \times J}$, and $\mathbf{B}_2 \in \mathbb{R}^{R \times J}$. Or equivalently, we can matricize \mathcal{C} into $\mathbf{C} \in \mathbb{R}^{IJ \times R_1 R_3}$ as follows,

$$\mathbf{C} = \text{diag}(\text{vec}(\mathbf{A}_3^\top \mathbf{B}_2)) (\mathbf{B}_1 \otimes \mathbf{A}_1)^\top.$$

The cherry product operation can be visually analogized to a tile-matching game: when two ‘‘cherry factors’’ are connected, they undergo a matrix multiplication, and the corresponding rank information is absorbed. Through a sequence of such cherry products, we can ultimately construct a tensor that has the same dimension as the original target tensor. This entire process formally defines the iFCTN decomposition, as presented below.

Definition 4 (iFCTN Decomposition). The iFCTN decomposition decomposes an N th-order tensor $\mathcal{X} \in \mathbb{R}^{I_1 \times I_2 \times \dots \times I_N}$ into a set of cherry tensors in Definition 2, which are composed of the corresponding cherry factors \mathbf{G}_k as in (3). Suppose the iFCTN-rank matrix $\mathbf{R} = (R_{i,j}) \in \mathbb{R}^{N \times N}$ is symmetric. Then, the element-wise form of the iFCTN decomposition can be expressed as follows,

$$\begin{aligned} & \mathcal{X}(i_1, i_2, \dots, i_N) \\ &= \sum_{r_{1,2}=1}^{R_{1,2}} \dots \sum_{r_{1,N}=1}^{R_{1,N}} \sum_{r_{2,3}=1}^{R_{2,3}} \dots \sum_{r_{2,N}=1}^{R_{2,N}} \dots \sum_{r_{N-1,N}=1}^{R_{N-1,N}} \\ & \{ \mathbf{G}_{1,2}(r_{1,2}, i_1) \mathbf{G}_{1,3}(r_{1,3}, i_1) \dots \mathbf{G}_{1,N}(r_{1,N}, i_1) \\ & \mathbf{G}_{2,1}(r_{1,2}, i_2) \mathbf{G}_{2,3}(r_{2,3}, i_2) \dots \mathbf{G}_{2,N}(r_{2,N}, i_2) \dots \\ & \mathbf{G}_{N,1}(r_{1,N}, I_N) \mathbf{G}_{N,2}(r_{2,N}, I_N) \dots \mathbf{G}_{N,N-1}(r_{N-1,N}, I_N) \}. \end{aligned} \quad (5)$$

We denote the iFCTN decomposition by

$$\mathcal{X} = \text{iFCTN} \left(\{\mathbf{G}_k\}_{k=1}^N \right) = \text{iFCTN} (\mathbf{G}_1, \dots, \mathbf{G}_N)$$

and call the vector collected by $\{R_{k_1, k_2}\} (k_1 < k_2)$ as the iFCTN-ranks.

Remark 2. In TN decompositions, such as TT, TR, FCTN, TW, every factor is a tensor of similar or lower order. Computing the k -th factor in a TN typically entails ‘‘packing’’ step that reformulates the remaining components into an effective sub-network. As illustrated in Fig. 2, the FCTN rebuilds an auxiliary sub-network at every iteration with repeated contractions, permutations, and folding/unfolding steps between the remaining tensors.

By contrast, all factors in iFCTN are matrices (‘‘cherries’’) and ‘‘packing’’ the remaining cherries into a sub-network can be explicitly represented with these matrices.

Proposition 1 (Mode- k Cherry Sub-network). Suppose that $\mathcal{X} = \text{iFCTN} \left(\{\mathbf{G}_t\}_{t=1}^N \right)$. Then, the cherry sub-network $\mathbf{Z}_k \in \mathbb{R}^{\prod_{i \in [N] \setminus k} I_i \times \prod_{i \in [N] \setminus k} R_{k,i}}$ comprises two components: (i) the cherry factors $\{\mathbf{G}_{t,i}\}_{i \neq t}$ for all $t \in [N] \setminus k$; (ii) the cherry factors \mathbf{G}_k . Specifically,

$$\mathbf{Z}_k = \text{diag}(\text{vec}(\mathcal{S}_k)) \times_{i \in \{N, \dots, 1\} \setminus k} \otimes \mathbf{G}_{i,k}^\top, \quad (6)$$

where \mathcal{S}_k is an $(N-1)$ th-order tensor shown as follows,

$$\mathcal{S}_k = \underset{i < j, i, j \in [N] \setminus k}{\circ} \left\{ \text{reshape} \left(\mathbf{G}_{i,j}^\top \mathbf{G}_{j,i}, [1, \dots, I_i, \dots, I_j, 1, \dots, 1] \right) \right\}.$$

Moreover, the mode- k unfolding of \mathcal{X} can be expressed by:

$$(\mathcal{X}_{(k)})^\top = \mathbf{Z}_k (\mathcal{G}_{(k)})^\top, \quad (7)$$

where $\mathcal{G}_{(k)} = \mathcal{CT}_k \left(\{\mathbf{G}_i\}_{i=1, i \neq k}^N \right)$.

4. iFCTN Decomposition-Based TC Method

In the following, the iFCTN decomposition method is employed to address the TC problem, with the aim of validating its rationality and superiority.

4.1. Model

Given an observation set Ω and an incomplete observation $\mathcal{O} \in \mathbb{R}^{I_1 \times I_2 \times \dots \times I_N}$, we aim to recover a target tensor \mathcal{X} that is low-rank within the iFCTN framework. Then, the proposed iFCTN-TC can be formulated as follows,

$$\min_{\mathcal{X}, \{\mathbf{G}_k\}_{k=1}^N} \frac{1}{2} \|\mathcal{X} - \text{iFCTN}(\mathbf{G}_1, \dots, \mathbf{G}_N)\|_F^2 + \iota(\mathcal{X}). \quad (8)$$

Here, $\iota(\mathcal{X})$ is an indicator function that enforces $\mathcal{X}(\mathbf{i}) = \mathcal{O}(\mathbf{i})$ for any $\mathbf{i} \in \Omega$ defined by

$$\iota(\mathcal{X}) := \begin{cases} 0, & \text{if } \mathcal{P}_\Omega(\mathcal{X}) = \mathcal{P}_\Omega(\mathcal{O}), \\ \infty, & \text{otherwise,} \end{cases}$$

where $\mathcal{P}_\Omega(\cdot)$ is a projection function. We also denote $\mathbf{G} := \{\mathbf{G}_k\}_{k=1}^N$, $f(\mathbf{G}, \mathcal{X}) = \frac{1}{2} \|\mathcal{X} - \text{iFCTN}(\mathbf{G}_1, \dots, \mathbf{G}_N)\|_F^2$, and $F(\mathbf{G}, \mathcal{X}) = \frac{1}{2} \|\mathcal{X} - \text{iFCTN}(\mathbf{G}_1, \dots, \mathbf{G}_N)\|_F^2 + \iota(\mathcal{X})$.

Although the objective function $F(\mathbf{G}, \mathcal{X})$ in (8) is non-convex, it is convex with respect to each block when the remaining blocks are fixed. Therefore, we employ the PAM scheme to iteratively update the variables as follows.

4.2. Algorithm

At the s -th iteration, we begin by sequentially updating the cherry factors for all $k \in [N]$ and $i \neq k$ as follows:

$$\mathbf{G}_{k,i}^{(s+1)} = \underset{\mathbf{G}_{k,i}}{\operatorname{argmin}} \left\{ f \left(\mathbf{G}_{<k,i}^{(s+1)}, \mathbf{G}_{k,i}^{(s)}, \mathbf{G}_{>k,i}^{(s)}, \mathcal{X}^{(s)} \right) + \frac{\rho}{2} \left\| \mathbf{G}_{k,i} - \mathbf{G}_{k,i}^{(s)} \right\|_F^2 \right\}.$$

Then, we update \mathcal{X} by:

$$\mathcal{X}^{(s+1)} = \underset{\mathcal{X}}{\operatorname{argmin}} \left\{ F \left(\mathbf{G}^{(s+1)}, \mathcal{X} \right) + \frac{\rho}{2} \left\| \mathcal{X} - \mathcal{X}^{(s)} \right\|_F^2 \right\}. \quad (9)$$

Here, $\rho > 0$ denotes the parameter controlling the proximal term, $\mathbf{G}_{<k,i}^{(s+1)} := \{\mathbf{G}_{1:k-1}^{(s+1)}, \mathbf{G}_{k,1:i-1}^{(s+1)}\}$, and $\mathbf{G}_{>k,i}^{(s)} := \{\mathbf{G}_{k,i+1:N}^{(s)}, \mathbf{G}_{k+1:N}^{(s)}\}$.

1) *Update $\mathbf{G}_{k,i}$* : According to Proposition 1, the $\mathbf{G}_{k,i}$ subproblem could be rewritten as follows,

$$\mathbf{G}_{k,i}^{(s+1)} = \underset{\mathbf{G}_{k,i}}{\operatorname{argmin}} \left\{ \frac{\rho}{2} \left\| \mathbf{G}_{k,i} - \mathbf{G}_{k,i}^{(s)} \right\|_F^2 + \left\| \mathbf{X}_{(k)}^\top - \mathbf{Z}_k^{(s)} \left(\mathbf{G}_{k,N}^{(s+1)} \odot \dots \odot \mathbf{G}_{k,i} \odot \dots \odot \mathbf{G}_{k,1}^{(s)} \right) \right\|_F^2 \right\}, \quad (10)$$

where $\mathbf{Z}_k^{(s)}$ is the k -th cherry subnetwork defined by (1). This is a linear least square over $\mathbf{G}_{k,i}$, which admits a closed-form solution. Since each column of $\mathbf{G}_{k,i}$ is separable in the subproblem, we therefore solve it column-wise to avoid constructing the large coefficient matrix explicitly. Specifically, for each $j \in [I_k]$, we could compute the j -th column of $\mathbf{G}_{k,i}$ as follows,

$$\begin{aligned} & \left(\mathbf{G}_{k,i}^{(s+1)} \right)_j \\ &= \left(\left(\mathbf{y}_j^\top \otimes \mathbf{G}_{i,k}^{(s)} \right) \mathbf{D}^2 \left(\mathbf{y}_j \otimes \mathbf{G}_{i,k}^{(s)\top} \right) + \rho \mathbf{I} \right)^{-1} \mathbf{b}_{i,k,j}, \end{aligned} \quad (11)$$

where $\mathbf{D} = \operatorname{diag}(\operatorname{vec}(\mathcal{S}))$, \mathbf{y}_j is the j -th column of $\mathbf{Y} = \bigodot_{m \neq i} \left(\mathbf{G}_{k,m}^{(s)\top} \mathbf{G}_{m,k}^{(s)} \right) \in \mathbb{R}^{(\prod_{m \neq i,k} I_m) \times I_k}$, and $\mathbf{b}_{i,k,j} = \left(\mathbf{y}_j^\top \otimes \mathbf{G}_{i,k}^{(s)} \right) \mathbf{D} \left(\mathbf{X}_k^\top \right)_j + \rho \left(\mathbf{G}_{k,i}^{(s)} \right)_j$.

2) *Update \mathcal{X}* : The loss function in (9) is completely separable across all elements of \mathcal{X} . Thus, for each index $i \in \Omega$, the update is fixed as $\mathcal{X}^{(s+1)}(\mathbf{i}) = \mathcal{O}(\mathbf{i})$; for all

other entries, it is updated by solving the corresponding least squares problem. This procedure yields the following closed-form solution:

$$\mathcal{X}^{(s+1)} = \mathcal{P}_{\Omega^c} \left(\frac{\text{iFCTN}(\mathbf{G})}{1 + \rho} + \rho \mathcal{X}^{(s)} \right) + \mathcal{P}_\Omega(\mathcal{O}). \quad (12)$$

Here, Ω^c denotes the complement of Ω .

The whole process of the PAM-based solver for iFCTN-TC is summarized in Algorithm 1.

Algorithm 1 A PAM-based solver for iFCTN-TC.

Input: The observed tensor $\mathcal{O} \in \mathbb{R}^{I_1 \times I_2 \times \dots \times I_N}$, the sample set Ω , the iFCTN-ranks $\mathbf{R} \in \mathbb{R}^{N \times N}$, ρ , t_{\max} , and ϵ .

Initialization: Set $s = 0$, $\mathcal{X}^{(0)} = \mathcal{O}$, and $\mathbf{G}_{k,i}^{(0)} \in \mathbb{R}^{R_{k,i} \times I_k}$.

- 1: **while** not converged and $s < t_{\max}$ **do**
- 2: **for** $k \in [N]$, $i \in [N] \setminus k$, and $j \in [I_k]$, **do**
- 3: Update $\left(\mathbf{G}_{k,i}^{(s+1)} \right)_j$ via (11).
- 4: **end for**
- 5: Update $\mathcal{X}^{(s+1)}$ via (12).
- 6: Check the convergence condition:

$$\left\| \mathcal{X}^{(s+1)} - \mathcal{X}^{(s)} \right\|_F / \left\| \mathcal{X}^{(s)} \right\|_F < \epsilon.$$

- 7: $s \leftarrow s + 1$
- 8: **end while**

Output: The recovered tensor \mathcal{X}

4.3. Complexity analysis

For simplicity, we assume that $\mathcal{X} \in \mathbb{R}^{I \times I \times \dots \times I}$ and $R_{k_1, k_2} = R_{k_2, k_1} = R$ for any $k_1, k_2 \in [N]$. We present a comparison between iFCTN and FCTN [29] in Table 1.

Storage complexity. In iFCTN, the $N(N-1)$ ‘‘cherries’’ each incur $\mathcal{O}(IR)$ memory, so the total storage scales as $\mathcal{O}(N(N-1)IR)$.

Computational complexity. (i) For each k and i , updating $G_{k,i}$ ($i \neq k$) in (11) involves the construction and solution of subproblems, which cost $\mathcal{O}(N^2(I^2R + I^{N-1}))$ and $\mathcal{O}(I^N + I^2R + IR^3)$. (ii) Updating \mathcal{X} from (12) requires $\mathcal{O}(I^N)$. Therefore, the whole computational complexity at each iteration in Algorithm 1 is $\mathcal{O}(NI^N + N^3I^{N-1} + N^3I^2R + NIR^3)$. In practice, the problem always operates in the regime $I \gg R > N$.

4.4. Convergence analysis

Under mild condition, we show that the sequence generated by Algorithm 1 globally converges to a critical point. The proof is detailed in the appendix.

Theorem 1. *Suppose that the sequence $\left\{ \left(\mathbf{G}^{(s)}, \mathcal{X}^{(s)} \right) \right\}$ obtained by the Algorithm 1 is bounded, then it globally converges to a critical point $(\mathbf{G}^*, \mathcal{X}^*)$ of $F(\mathbf{G}, \mathcal{X})$.*

Table 1. Storage and computational complexity comparison between FCTN and iFCTN (ours) for 3rd and N -th order tensors. Here, we assume that $I = I_1 = \dots = I_N$ and $R = R_{ij}$ for any $i, j \in [N]$.

Order	Method	Storage complexity	Computation complexity
3-D	FCTN	$\mathcal{O}(IR^2)$	$\mathcal{O}(I^3R^2)$
	iFCTN	$\mathcal{O}(IR)$	$\mathcal{O}(I^3)$
N -D	FCTN	$\mathcal{O}(NIR^{N-1})$	$\mathcal{O}\left(N \sum_{k=2}^N I^k R^{k(N-k)+k-1} + NI^{N-1}R^{2(N-1)} + NR^{3(N-1)}\right)$
	iFCTN	$\mathcal{O}(N(N-1)IR)$	$\mathcal{O}(NI^N + N^3I^{N-1} + N^3I^2R + NIR^3)$

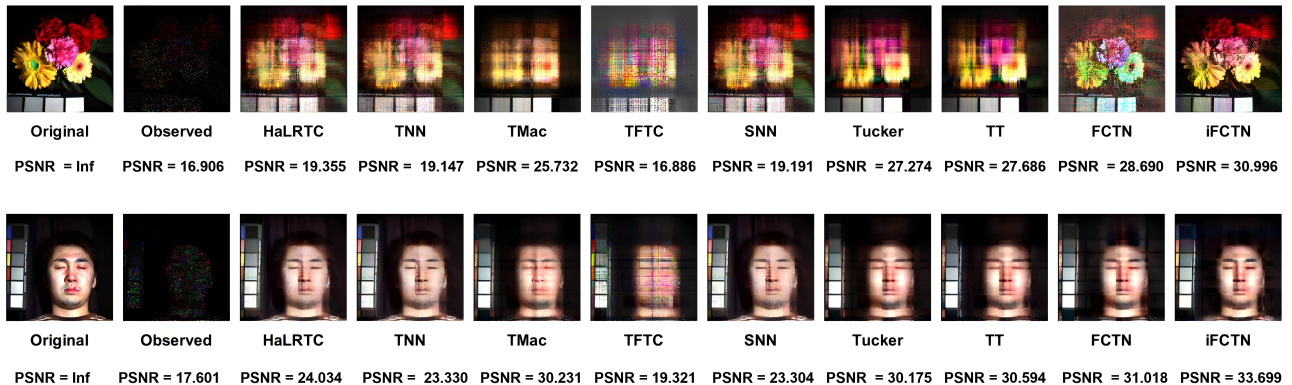


Figure 3. The pseudo-color renderings of reconstructions (composed of the 29th, 19th, and 9th bands) and corresponding PSNRs for MSI datasets. The first row is *flower* with RM = 90%, the second row is *face* with RM = 80%.

5. Experiments

Extensive numerical experiments were conducted to evaluate the effectiveness of the proposed iFCTN-TC method with different random-missing (RM) and fiber-missing (FM) levels. The algorithm parameters were set as follows: the proximal parameter $\rho = 0.1$, maximum iteration $t_{\max} = 1000$, and stopping criteria $\epsilon = 10^{-5}$. All simulations implemented in MATLAB on a computer of 12th Gen Intel(R) Core(TM) i7-12700H (20 CPUs), 2.3GHz. We compare iFCTN against eight state-of-the-art baselines: HaLRTC [12], TNN [25], TMac [23], TFTC [31], SNN [12], Tucker [19], TT [16], and FCTN [29].

5.1. Multispectral images

We first evaluate three MSI data (*face*, *toy*, *flower*) from CAVE², each of size $256 \times 256 \times 31$ (spatial height \times spatial width \times bands). For iFCTN-TC, we set $R_{1,2} \in \{3, 6, 9, 15, 30, 36\}$ and $R_{1,3} = R_{2,3} \in \{3, 6, 9\}$. For FCTN-TC, we likewise set $R_{1,2} \in \{2, 3, 6, 9, 15, 30, 36\}$ and $R_{1,3} = R_{2,3} \in \{3, 6, 9, 12\}$. For TT-TC and Tucker-TC rank, we select ranks element from $\{2, 3, 6, 9, 12, 15\}$. We report the best performance overall all rank selections.

²<http://www.cs.columbia.edu/CAVE/databases>. The results for the *toy* dataset are provided in the appendix due to space constraints.

For evaluation, we report peak signal-to-noise ratio (PSNR), structural similarity (SSIM) [22], relative error (RSE), i.e. $RSE = \|\mathcal{X}_{true} - \mathcal{X}\|_F / \|\mathcal{X}\|_F$, the root mean square error (RMSE), i.e. $RMSE = \sqrt{\frac{1}{T} \|\mathcal{X}_{true} - \mathcal{X}\|_F^2}$, and total CPU time in seconds (includes the time required to tune all parameters) are used to evaluate model performance. Here, T is the total number of missing entries.

Fig. 3 presents the reconstruction results and the corresponding PSNRs for *flower* and *face*. We observe that iFCTN is robust and efficient. For instance, on both *flower* and *face*, its PSNR exceeds the second-best result by 2.5 dB. Due to space limitations, we place the results corresponding to *Toy* in the supplementary materials.

We continue to present the results over fiber missing in terms of bands³ in Table 2. The PSNR and SSIM outcomes are similar to those shown in Fig. 3. For instance, iFCTN-TC exceeds the second-best method by 3 dB in PSNR at FM = 60% for *face*, and by 1.5 dB in PSNR at FM = 70% for *flower*. Note that although our theoretical analysis shows much lower computational complexity, the increased CPU time, as compared to matrix-updated networks such as FCTN, is mainly due to the structure of the update rule

³Owing to space limitations, we place the results in terms of random missing comparison to the supplementary materials.

Table 2. Results of PSNR, SSIM, and runtime for *face and flower* under different fiber missing ratios (FR). The best results are highlighted in **bold**; the second-best are underlined.

Dataset	method	80%			70%			60%			50%		
		PSNR	SSIM	time (s)									
<i>flower</i>	Observed	17.455	0.483	—	17.999	0.536	—	18.651	0.583	—	19.481	0.632	—
	HaLRTC	19.870	0.628	22.105	21.685	0.695	23.040	23.098	0.761	22.777	27.026	0.834	22.928
	TNN	19.681	0.623	267.580	21.376	0.687	266.393	23.503	0.751	259.588	26.289	0.821	262.842
	TMac	24.413	0.640	2.376	26.106	0.682	2.508	27.595	0.725	2.935	30.294	0.774	2.197
	TFTC	25.811	0.625	27.052	26.598	0.671	15.014	27.451	0.705	10.565	28.335	0.748	7.345
	SNN	20.043	0.628	275.032	21.928	0.697	287.197	24.333	0.766	293.600	27.513	0.840	271.044
	Tucker	26.027	0.643	6.864	26.818	0.685	5.424	27.635	0.720	4.442	28.653	0.756	2.302
	TT	<u>26.476</u>	<u>0.655</u>	19.843	27.329	0.700	12.195	29.045	0.735	7.727	30.174	0.773	4.393
	FCTN	25.105	0.595	38.644	<u>27.445</u>	<u>0.699</u>	35.631	<u>29.195</u>	<u>0.749</u>	14.592	<u>30.071</u>	<u>0.776</u>	23.456
	Ours	26.825	0.681	77.789	28.987	0.755	64.107	30.243	0.795	25.553	31.196	0.827	27.619
<i>face</i>	Observed	17.620	0.411	—	18.176	0.472	—	18.902	0.526	—	19.682	0.578	—
	HaLRTC	20.380	0.659	22.515	22.483	0.721	24.091	25.451	0.789	24.293	29.222	0.856	37.215
	TNN	20.158	0.653	277.910	22.105	0.712	277.699	24.807	0.776	273.502	28.143	0.838	402.898
	TMac	19.231	0.526	2.245	22.094	0.656	2.511	25.459	0.740	3.272	29.734	0.826	3.929
	TFTC	29.882	0.778	78.462	31.812	0.819	44.604	31.828	0.845	17.545	32.640	0.873	10.857
	SNN	17.960	0.507	277.402	22.754	0.726	289.055	25.878	0.796	287.169	29.899	0.865	405.575
	Tucker	29.572	0.778	11.964	30.422	0.816	2.619	31.207	0.844	1.653	32.010	0.870	1.738
	TT	29.869	0.785	29.788	30.779	0.824	8.037	31.566	0.852	4.424	32.316	0.877	3.862
	FCTN	<u>30.126</u>	<u>0.790</u>	18.415	<u>31.122</u>	<u>0.815</u>	11.521	<u>31.282</u>	<u>0.837</u>	13.812	<u>32.876</u>	<u>0.873</u>	10.857
	Ours	31.243	0.832	71.735	33.121	0.881	35.685	34.316	0.904	14.214	35.154	0.920	12.610

*Although the computational complexity of iFCTN is much lower than FCTN, the closed-form update in (11) relies on extensive ‘for’ loops (over $k, i,$ and j), which are inefficient in MATLAB, leading to longer actual CPU time.

in (11). The closed-form solution involves iterating over multiple indices (k, i, j) via ‘for’ loops, a process that is slow in interpreted languages like MATLAB, despite a manageable theoretical computational complexity.

5.2. Traffic data

We further evaluate iFCTN-TC on two traffic datasets: 1) *Guangzhou*⁴ contains travel speed observations from 214 road segments in two months (61 days from August 1, 2016 to September 30, 2016) at 10 min interval (144 time intervals in a day), whose size is $214 \times 61 \times 144$ (road segment \times day \times time interval); 2) *Birmingham*⁵ is collected from 18 Car park ID in two months (October 4, 2016 to December 19, 2016) at 30 min interval, whose size is $30 \times 77 \times 18$ (time interval \times day \times zone).

For iFCTN-TC, we set $R_{1,2} \in \{2, 3, 4, 6, 9, 12, 36\}$ and $R_{1,3} = R_{2,3} \in \{3, 6, 9, 12\}$. For FCTN-TC, we set $R_{1,3} = R_{2,3} \in \{2, 3, 6, 9, 15, 36\}$ and $R_{1,3} \in \{3, 6, 9, 12\}$. For TT-TC and Tucker-TC rank, we select ranks from $\{2, 3, 6, 9\}$.

In Fig. 4, we present the FM reconstruction results at the 1st day and the RSE over the entire datasets. These results demonstrate the superiority of the iFCTN decomposi-

tion for the FM settings⁶. Table 3 shows iFCTN-TC attains the best performance in most cases.

6. Conclusion

We have presented intra-block FCTN (iFCTN), an (un)folding-free reformulation of the fully connected tensor network decomposition. By decomposing the tensor factors into matrix factors with the KR product, iFCTN eliminates the expensive auxiliary subnetworks reconstruction that burdens standard FCTN. When applied to the TC problem, the proposed PAM algorithm exhibits provable convergence, along with favorable reconstruction accuracy and robust performance. Extensive experiments on public data show that iFCTN delivers state-of-the-art recovery results.

Limitations. Similar to CP, TR, and FCTN decompositions [11, 26, 29], the proposed iFCTN decomposition faces a difficult rank-selection problem. In the future, we will develop principled strategies for rank determination and extend iFCTN to online, large-scale, and higher-order scenarios.

⁴<https://doi.org/10.5281/zenodo.1205229>

⁵<https://archive.ics.uci.edu/dataset/482/parking+birmingham>

⁶Figures for random missing and tables for fiber missing are deferred to the supplementary material.

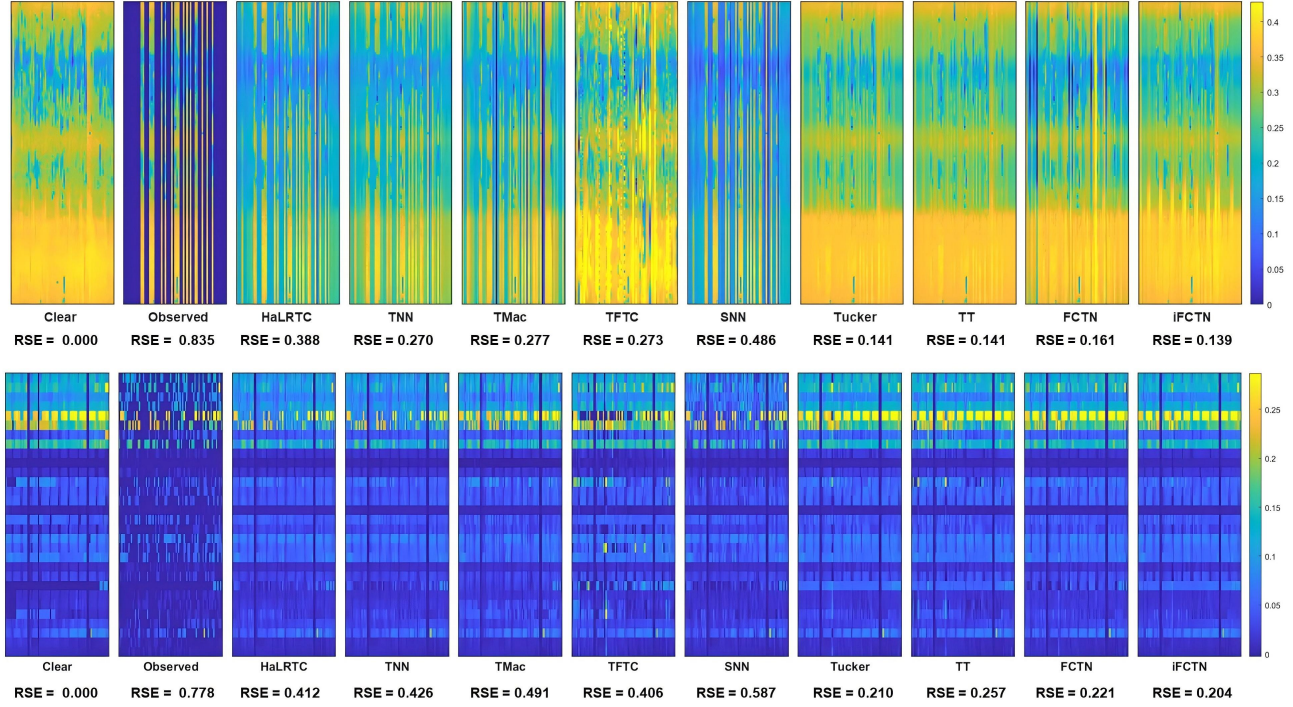


Figure 4. Reconstructions on Day 1. The first row is *Guangzhou* with FM = 70% and the second row is *Birmingham* with FM = 60%.

Table 3. Performance on RSE, RMSE, and CPU time for *Guangzhou* and *Birmingham* under different random missing ratios. The best results are highlighted in **bold**; the second-best are underlined.

Dataset	method	99%			95%			90%			80%		
		RSE	RMSE	time (s)									
<i>Guangzhou</i>	Observed	0.995	0.337	—	0.975	0.337	—	0.949	0.337	—	0.895	0.337	—
	HaLRTC	0.992	0.336	10.925	0.962	0.333	11.864	0.928	0.330	12.556	0.863	0.325	12.722
	TNN	0.351	0.119	180.560	0.162	0.056	20.693	0.144	0.051	14.750	0.129	0.049	11.044
	TMac	0.691	0.234	1.225	0.181	0.063	1.369	0.145	0.051	1.740	0.141	0.053	2.046
	TFTC	0.970	0.329	27.439	1.060	0.367	83.514	1.046	0.372	90.963	0.711	0.268	99.164
	SNN	0.993	0.336	179.336	0.964	0.334	188.840	0.932	0.331	194.388	0.869	0.327	195.137
	Tucker	0.229	0.078	22.786	<u>0.141</u>	<u>0.049</u>	25.091	<u>0.133</u>	<u>0.047</u>	26.349	0.117	0.044	26.975
	TT	0.346	0.117	59.209	0.158	0.055	59.704	0.135	0.048	62.390	0.129	0.048	18.176
	FCTN	<u>0.194</u>	<u>0.066</u>	15.844	0.152	0.052	33.741	0.150	0.053	73.221	<u>0.106</u>	<u>0.040</u>	71.839
	Ours	0.178	0.060	72.732	0.120	0.042	52.976	0.113	0.040	70.169	0.104	0.039	56.559
<i>Birmingham</i>	Observed	0.996	0.197	—	0.970	0.195	—	0.946	0.195	—	0.893	0.193	—
	HaLRTC	0.996	0.197	0.007	0.730	0.147	0.563	0.394	0.081	0.563	0.774	0.033	0.420
	TNN	0.996	0.197	0.008	0.462	0.093	0.991	0.250	0.052	0.895	0.154	0.033	0.629
	TMac	1.021	0.202	0.042	0.455	0.091	0.043	0.272	0.056	0.049	<u>0.149</u>	<u>0.032</u>	0.053
	TFTC	0.992	0.196	0.799	0.965	0.194	1.750	1.111	0.229	2.057	1.164	0.282	2.045
	SNN	0.993	0.196	0.876	0.480	0.097	5.164	0.235	0.048	5.333	0.558	0.121	3.981
	Tucker	0.722	0.143	0.949	0.414	0.083	1.103	0.230	0.047	1.265	0.170	0.037	0.675
	TT	0.805	0.159	1.534	<u>0.281</u>	<u>0.056</u>	1.559	<u>0.189</u>	<u>0.039</u>	1.243	0.175	0.038	0.533
	FCTN	0.800	0.158	0.969	0.430	0.086	1.022	0.239	0.049	1.049	0.156	0.034	1.201
	Ours	<u>0.739</u>	<u>0.146</u>	2.679	0.192	0.039	2.729	0.177	0.036	2.059	0.145	0.031	1.675

*Although the computational complexity of iFCTN is much lower than FCTN, the closed-form update in (11) relies on extensive ‘for’ loops (over k , i , and j), which are inefficient in MATLAB, leading to longer actual CPU time.

References

- [1] Animashree Anandkumar, Rong Ge, Daniel J Hsu, Sham M Kakade, Matus Telgarsky, et al. Tensor decompositions for learning latent variable models. *Journal of Machine Learning Research*, 15(1):2773–2832, 2014. 1
- [2] Grey Ballard and Tamara G. Kolda. *Tensor decompositions for data science*. Cambridge University Press, 2025. 1
- [3] Johann A. Bengua, Ho N. Phien, Hoang Duong Tuan, and Minh N. Do. Efficient tensor completion for color image and video recovery: low-rank tensor train. *IEEE Transactions on Image Processing*, 26(5):2466–2479, 2017. 1
- [4] Andrzej Cichocki, Rafal Zdunek, Anh-Huy Phan, and Shun-ichi Amari. *Nonnegative matrix and tensor factorizations*, chapter 7, pages 337–432. John Wiley & Sons, Ltd, 2009. 1
- [5] Andrzej Cichocki, Danilo Mandic, Anh-Huy Phan, Cesar Caiafa, Guoxu Zhou, Qibin Zhao, and Lieven Lathauwer. Tensor decompositions for signal processing applications from two-way to multiway component analysis. *Signal Processing Magazine, IEEE*, 32, 2014. 1
- [6] Zhi-Long Han, Ting-Zhu Huang, Xi-Le Zhao, Hao Zhang, and Wei-Hao Wu. Nested fully-connected tensor network decomposition for multi-dimensional visual data recovery. *IEEE Transactions on Circuits and Systems for Video Technology*, 34(10):10092–10106, 2024. 1
- [7] Frank L. Hitchcock. The expression of a tensor or a polyadic as a sum of products. *Journal of Mathematics and Physics*, 6(1-4):164–189, 1927. 1
- [8] Wei-Jian Huang, Li Huang, Tai-Xiang Jiang, Yu-Bang Zheng, and Guisong Liu. Efficient FCTN decomposition with structural sparsity for noisy tensor completion. *IEEE Transactions on Big Data*, 2025. 1
- [9] Behnoush Khavari and Guillaume Rabusseau. Lower and upper bounds on the pseudo-dimension of tensor network models. In *Advances in Neural Information Processing Systems*, pages 10931–10943. Curran Associates, Inc., 2021. 1
- [10] Misha E Kilmer, Karen Braman, Ning Hao, and Robert C Hoover. Third-order tensors as operators on matrices. *SIAM Journal on Matrix Analysis and Applications*, 34(1):148–172, 2013. 1
- [11] Tamara G Kolda and Brett W Bader. Tensor decompositions and applications. *SIAM Review*, 51(3):455–500, 2009. 1, 7
- [12] Ji Liu, Przemyslaw Musialski, Peter Wonka, and Jieping Ye. Tensor completion for estimating missing values in visual data. *IEEE Transactions on Pattern Analysis and Machine Intelligence*, 35(1):208–220, 2013. 6
- [13] Yun-Yang Liu, Xi-Le Zhao, Guang-Jing Song, Yu-Bang Zheng, Michael K. Ng, and Ting-Zhu Huang. Fully-connected tensor network decomposition for robust tensor completion problem. *Inverse Problems and Imaging*, 18(1):208–238, 2024. 1
- [14] Yun-Yang Liu, Xi-Le Zhao, and Gemine Vivone. Rank-revealing fully-connected tensor network decomposition and its application to tensor completion. *Pattern Recognition*, 165:111610, 2025. 1
- [15] Cheng-Yao Lyu, Xi-Le Zhao, Ben-Zheng Li, Hao Zhang, and Ting-Zhu Huang. Multi-dimensional image recovery via fully-connected tensor network decomposition under the learnable transforms. *Journal of Scientific Computing*, 93(2):49, 2022. 1
- [16] Ivan V Oseledets. Tensor-train decomposition. *SIAM Journal on Scientific Computing*, 33(5):2295–2317, 2011. 1, 6
- [17] Nicholas D Sidiropoulos, Lieven De Lathauwer, Xiao Fu, Kejun Huang, Evangelos E Papalexakis, and Christos Faloutsos. Tensor decomposition for signal processing and machine learning. *IEEE Transactions on signal processing*, 65(13):3551–3582, 2017. 1
- [18] Ruoyang Su, Xi-Le Zhao, Wei-Hao Wu, Sheng Liu, and Junhua He. Deep fully-connected tensor network decomposition for multi-dimensional signal recovery. *Signal Processing*, 233:109903, 2025. 2
- [19] Ledyard R Tucker. Some mathematical notes on three-mode factor analysis. *Psychometrika*, 31(3):279–311, 1966. 1, 6
- [20] Mengyu Wang, Honghua Cui, and Hanyu Li. A random sampling algorithm for fully-connected tensor network decomposition with applications. *Computational and Applied Mathematics*, 43(4):226, 2024. 1, 2
- [21] Wenqi Wang, Yifan Sun, Brian Eriksson, Wenlin Wang, and Vaneet Aggarwal. Wide compression: tensor ring nets. In *Proceedings of the IEEE conference on computer vision and pattern recognition*, pages 9329–9338, 2018. 1
- [22] Zhou Wang, Alan C Bovik, Hamid R Sheikh, and Eero P Simoncelli. Image quality assessment: from error visibility to structural similarity. *IEEE transactions on image processing*, 13(4):600–612, 2004. 6
- [23] Yangyang Xu, Ruru Hao, Wotao Yin, and Zhixun Su. Parallel matrix factorization for low-rank tensor completion. *Inverse Problems and Imaging*, 9(2):601–624, 2015. 6
- [24] Jinshi Yu, Zhifu Li, Ge Ma, Jingwen Wang, Tao Zou, and Guoxu Zhou. Low-rank sparse fully-connected tensor network for tensor completion. *Pattern Recognition*, 158:111000, 2025. 1
- [25] Zemin Zhang, Gregory Ely, Shuchin Aeron, Ning Hao, and Misha Kilmer. Novel methods for multilinear data completion and de-noising based on tensor-svd. In *Proceedings of the IEEE conference on computer vision and pattern recognition*, pages 3842–3849, 2014. 6
- [26] Qibin Zhao, Guoxu Zhou, Shengli Xie, Liqing Zhang, and Andrzej Cichocki. Tensor ring decomposition. *arXiv preprint arXiv:1606.05535*, 2016. 1, 7
- [27] Wen-Jie Zheng, Xi-Le Zhao, Yu-Bang Zheng, and Zhi-Feng Pang. Nonlocal patch-based fully connected tensor network decomposition for multispectral image inpainting. *IEEE Geoscience and Remote Sensing Letters*, 19:1–5, 2021. 1
- [28] Wen-Jie Zheng, Xi-Le Zhao, Yu-Bang Zheng, and Ting-Zhu Huang. Provable stochastic algorithm for large-scale fully-connected tensor network decomposition. *Journal of Scientific Computing*, 98(1):16, 2024. 1, 2
- [29] Yu-Bang Zheng, Ting-Zhu Huang, Xi-Le Zhao, Qibin Zhao, and Tai-Xiang Jiang. Fully-connected tensor network decomposition and its application to higher-order tensor completion. In *Proceedings of the AAAI conference on artificial intelligence*, pages 11071–11078, 2021. 1, 2, 5, 6, 7
- [30] Yu-Bang Zheng, Xi-Le Zhao, Junhua Zeng, Chao Li, Qibin Zhao, Heng-Chao Li, and Ting-Zhu Huang. SVDinsTN:

A tensor network paradigm for efficient structure search from regularized modeling perspective. In *Proceedings of the IEEE/CVF conference on computer vision and pattern recognition*, pages 26254–26263, 2024. 1

- [31] Pan Zhou, Canyi Lu, Zhouchen Lin, and Chao Zhang. Tensor factorization for low-rank tensor completion. *IEEE Transactions on Image Processing*, 27(3):1152–1163, 2018. 6

iFCTN: Folding-Free Fully-Connected Tensor Network Decomposition for Tensor Completion

Supplementary Material

1. Proof of Proposition 1

Proposition 1 (Mode- k Cherry Sub-network). *Suppose that $\mathcal{X} = \text{iFCTN}(\{\mathbf{G}_t\}_{t=1}^N)$. Then, the cherry sub-network $\mathbf{Z}_k \in \mathbb{R}^{\prod_{i \in [N] \setminus k} I_i \times \prod_{i \in [N] \setminus k} R_{k,i}}$ comprises two components: (i) the cherry factors $\{\mathbf{G}_{t,i}\}_{i \neq t}$ for all $t \in [N] \setminus k$; (ii) the cherry factors \mathbf{G}_k . Specifically,*

$$\mathbf{Z}_k = \text{diag}(\text{vec}(\mathcal{S}_k)) \times_{i \in \{N, \dots, 1\} \setminus k} \otimes \mathbf{G}_{i,k}^\top, \quad (1)$$

where \mathcal{S}_k is an $(N-1)$ th-order tensor shown as follows,

$$\mathcal{S}_k = \underset{i < j, i, j \in [N] \setminus k}{\circ} \left\{ \text{reshape}(\mathbf{G}_{i,j}^\top \mathbf{G}_{j,i}, [1, \dots, I_i, \dots, I_j, 1, \dots, 1]) \right\}.$$

Moreover, the mode- k unfolding of \mathcal{X} can be expressed by:

$$(\mathcal{X}_{(k)})^\top = \mathbf{Z}_k (\mathcal{G}_{(k)})^\top, \quad (2)$$

where $\mathcal{G}_{(k)} = \mathcal{CT}_k(\{\mathbf{G}_i\}_{i=1, i \neq k}^N)$.

Proof. According to the definition of cherry product, $\mathcal{Z}_k = \text{iFCTN}(\mathbf{G}_1, \dots, \mathbf{G}_{k-1}, \mathbf{G}_{k+1}, \dots, \mathbf{G}_N)$ is of size $(I_1, R_{1,k}, \dots, I_{k-1}, R_{k-1,k}, R_{k+1,k}, I_{k+1}, \dots, R_{N,k}, I_N)$ and is given by

$$\begin{aligned} & \mathcal{Z}_k(i_1, r_{1,k}, \dots, i_{k-1}, r_{k-1,k}, r_{k+1,k}, i_{k+1}, \dots, r_{N,k}, i_N) \\ &= \prod_{m=1}^{k-1} \mathbf{G}_{m,k}(r_{m,k}, i_m) \prod_{n=k+1}^N \mathbf{G}_{n,k}(r_{n,k}, i_n) \\ & \left(\sum_{j \in [N] \setminus k} \sum_{i < j} \mathbf{G}_{i,j}^\top \mathbf{G}_{j,i} \right)_{I_i, I_j} \\ &= \prod_{m=1}^{k-1} \mathbf{G}_{m,k}(r_{m,k}, i_m) \prod_{n=k+1}^N \mathbf{G}_{n,k}(r_{n,k}, i_n) \\ & \mathcal{S}_k(i_{1:k-1}, i_{k+1:N}), \end{aligned} \quad (3)$$

where $\mathcal{S}_k(i_{1:k-1}, i_{k+1:N}) \in \mathbb{R}^{\prod_{i \neq k} I_i \times \prod_{i \neq k} R_{k,i}}$ is defined as

$$\mathcal{S}_k = \underset{i < j, i, j \in [N] \setminus k}{\circ} \left\{ \text{reshape}(\mathbf{G}_{i,j}^\top \mathbf{G}_{j,i}, [1, \dots, I_i, \dots, I_j, 1, \dots, 1]) \right\}.$$

Perform a generalized matricization of the tensor \mathcal{Z}_k to obtain \mathbf{Z}_k^\top , in which all modes $\{R_i\}_{i \neq k}$ are arranged row-

wise and all modes $\{I_i\}_{i \neq k}$ are column-wise.

$$\begin{aligned} & \mathbf{Z}_k^\top((r_{1:k-1,k}, r_{k+1:N,k}), (I_{1:k-1}, I_{k+1:N})) \\ &= \mathcal{Z}_k(i_1, r_{1,k}, \dots, i_{k-1}, r_{k-1,k}, r_{k+1,k}, i_{k+1}, \dots, r_{N,k}, i_N). \end{aligned} \quad (4)$$

Since the Kronecker product \otimes naturally captures the structure of this combined indexing, we have

$$\mathbf{K}(:, \text{col}(i_{1:k-1}, i_{k+1:N})) = \underset{i \in \{N, \dots, 1\} \setminus k}{\otimes} \mathbf{G}_{i,k}. \quad (5)$$

This implies that in the matrix \mathbf{Z}_k^\top , the column indexed by $(I_1, \dots, I_{k-1}, I_{k+1}, \dots, I_N)$ can be expressed as:

$$\begin{aligned} & \mathbf{Z}_k^\top(:, (i_{1:k-1}, i_{k+1:N})) \\ &= \mathcal{S}_k(i_{1:k-1}, i_{k+1:N}) \times \mathbf{K}(:, \text{col}(i_{1:k-1}, i_{k+1:N})) \end{aligned} \quad (6)$$

Therefore, the entire matrix \mathbf{Z}_k^\top can be expressed as:

$$\mathbf{Z}_k^\top = \underset{i \in \{N, \dots, 1\} \setminus k}{\otimes} \mathbf{G}_{i,k} \times \text{diag}(\text{vec}(\mathcal{S}_k)), \quad (7)$$

Namely,

$$\mathbf{Z}_k = \text{diag}(\text{vec}(\mathcal{S}_k)) \times_{i \in \{N, \dots, 1\} \setminus k} \otimes \mathbf{G}_{i,k}^\top,$$

Given the expression for \mathbf{Z}_k , it is straightforward to obtain the expansion for the mode- k unfolding of \mathcal{X} :

$$(\mathcal{X}_{(k)})^\top = \mathbf{Z}_k (\mathcal{G}_{(k)})^\top.$$

where $\mathcal{G}_{(k)} = \mathcal{CT}_k(\{\mathbf{G}_i\}_{i=1, i \neq k}^N)$.

The proof is completed. \square

2. Proof of Theorem 1

Before proving Theorem 1, we first rewrite the proposed iFCTN-TC model as follows,

$$\min_{\mathcal{M}} F(\mathcal{M}) = f(\mathcal{M}) + h(\mathcal{X}), \quad (8)$$

where $\mathcal{M} = (\mathbf{G}, \mathcal{X})$, $f(\mathcal{M}) = \frac{1}{2} \|\mathcal{X} - \text{iFCTN}(\mathbf{G}_1, \dots, \mathbf{G}_N)\|_F^2$, and $h(\mathcal{X}) = \iota(\mathcal{X})$.

Theorem 1. *Suppose that the sequence $\left\{ \left(\mathbf{G}^{(s)}, \mathcal{X}^{(s)} \right) \right\}$ obtained by the Algorithm 1 is bounded, then it globally converges to a critical point $(\mathbf{G}^*, \mathcal{X}^*)$ of $F(\mathbf{G}, \mathcal{X})$.*

Proof. According to the finite length property [1], the bounded sequence $\{\mathcal{M}^{(s)}\}_{s \in \mathbb{N}}$ could converge to the critical point when the following three lemmas are satisfied. \square

Lemma 1. *The objective function $F(\mathcal{M})$ in problem (8) is a Kurdyka-Łojasiewicz (KL) function.*

Proof. Following [1, 2], since $f(\mathcal{M})$ is a polynomial function of $N(N-1)+1$ coupling variations, it is an obviously real-analytic function. Regarding $h(\mathcal{X})$, since the constraint set $\{\mathcal{X} : \mathcal{P}_\Omega(\mathcal{X}) = \mathcal{P}_\Omega(\mathcal{O})\}$ is semi-algebraic, $\iota(\mathcal{X})$ is a semi-algebraic function. Therefore, $F(\mathcal{M})$, as a finite sum of real-valued analytic and semi-algebraic functions, is a KL function. \square

Lemma 2. [Sufficient decrease] *Let $\{\mathcal{M}^{(s)}\}_{s \in \mathbb{N}}$ be a sequence generated by Algorithm 1. Then, the sequence explicitly satisfies*

$$F(\mathcal{M}^{(s)}) - F(\mathcal{M}^{(s+1)}) \geq \frac{\rho}{2} \left\| \mathcal{M}^{(s+1)} - \mathcal{M}^{(s)} \right\|_F^2,$$

$$\text{where } \left\| \mathcal{M}^{(s+1)} - \mathcal{M}^{(s)} \right\|_F^2 = \left\| \mathcal{X}^{(s+1)} - \mathcal{X}^{(s)} \right\|_F^2 + \sum_{k=1}^N \sum_{i \neq k}^N \left\| \mathbf{G}_{k,i}^{(s+1)} - \mathbf{G}_{k,i}^{(s)} \right\|_F^2.$$

Proof. By the update scheme of $\{\mathbf{G}_{k,i}^{(s)}\}$, $k \in [N]$ and $i \in [N] \setminus k$, we have

$$\begin{aligned} & f\left(\mathbf{G}_{<k,i}^{(s+1)}, \mathbf{G}_{k,i}^{(s+1)}, \mathbf{G}_{>k,i}^{(s)}, \mathcal{X}^{(s)}\right) + \frac{\rho}{2} \left\| \mathbf{G}_{k,i}^{(s+1)} - \mathbf{G}_{k,i}^{(s)} \right\|_F^2 \\ & \leq f\left(\mathbf{G}_{<k,i}^{(s+1)}, \mathbf{G}_{k,i}^{(s)}, \mathbf{G}_{>k,i}^{(s)}, \mathcal{X}^{(s)}\right). \end{aligned} \quad (9)$$

Likewise, it follows from the update scheme of \mathcal{X} that

$$\begin{aligned} & f\left(\mathbf{G}^{(s+1)}, \mathcal{X}^{(s+1)}\right) + \frac{\rho}{2} \left\| \mathcal{X}^{(s+1)} - \mathcal{X}^{(s)} \right\|_F^2 \\ & \leq f\left(\mathbf{G}^{(s+1)}, \mathcal{X}^{(s)}\right). \end{aligned} \quad (10)$$

Finally, by taking summation over (9) and (10) and eliminating the duplicates, we can deduce

$$\begin{aligned} & F(\mathcal{M}^{(s)}) - F(\mathcal{M}^{(s+1)}) \\ & \geq \frac{\rho}{2} \left\| \mathcal{X}^{(s+1)} - \mathcal{X}^{(s)} \right\|_F^2 + \sum_{k=1}^N \sum_{i \neq k}^N \frac{\rho}{2} \left\| \mathbf{G}_{k,i}^{(s+1)} - \mathbf{G}_{k,i}^{(s)} \right\|_F^2. \end{aligned}$$

The proof is completed. \square

Lemma 3 (Relative Error Condition). *Let $\{\mathcal{M}^{(s)}\}$ be a bounded sequence generated by Algorithm 1. Then, there exists $\mathcal{P}^{(s+1)} \in \partial F(\mathcal{M}^{(s+1)})$ such that*

$$\left\| \mathcal{P}^{(s+1)} \right\|_F \leq L_F \left\| \mathcal{M}^{(s+1)} - \mathcal{M}^{(s)} \right\|_F,$$

where $L_F = N(N-1)\rho + \sum_{k=1}^N \sum_{i \neq k}^N L_{k,i}$. Here, $L_{k,i}$ denotes the gradient's Lipschitz constant of $F(\mathbf{G}, \mathcal{X})$ with respect to $G_{k,i}$.

Proof. According to the proof of Lemma 2, $\mathbf{G}^{(s+1)}$ and $\mathcal{X}^{(s+1)}$ are the minimum solutions, thus we have $h(\mathcal{X}^{(s+1)}) \equiv 0$ for avoiding $F(\mathcal{M}) \rightarrow 0$. According to the fact that minimum solutions must satisfy the first-order optimal conditions, i.e., the sub-gradient equations of the objective function, then for all $s \in \mathbb{N}$, we always have

$$\begin{cases} 0 \in \partial_{\mathbf{G}_{k,i}} f\left(\mathbf{G}_{<k,i}^{(s+1)}, \mathbf{G}_{k,i}^{(s+1)}, \mathbf{G}_{>k,i}^{(s)}, \mathcal{X}^{(s)}\right) + \rho(\mathbf{G}_{k,i}^{(s+1)} - \mathbf{G}_{k,i}^{(s)}), \\ 0 \in \partial_{\mathcal{X}} f(\mathbf{G}^{(s+1)}, \mathcal{X}^{(s+1)}) + \rho(\mathcal{X}^{(s+1)} - \mathcal{X}^{(s)}). \end{cases} \quad (11)$$

Based on the sub-differentiability property, we have

$$\partial F(\mathcal{M}^{(s+1)}) = \left(\partial_{\mathbf{G}} F(\mathbf{G}^{(s+1)}, \mathcal{X}^{(s+1)}), \partial_{\mathcal{X}} F(\mathbf{G}^{(s+1)}, \mathcal{X}^{(s+1)}) \right), \quad (12)$$

where

$$\begin{cases} \partial_{\mathbf{G}} F(\mathbf{G}^{(s+1)}, \mathcal{X}^{(s+1)}) = \partial_{\mathbf{G}} f(\mathbf{G}^{(s+1)}, \mathcal{X}^{(s+1)}), \\ \partial_{\mathcal{X}} F(\mathbf{G}^{(s+1)}, \mathcal{X}^{(s+1)}) = \partial_{\mathcal{X}} f(\mathbf{G}^{(s+1)}, \mathcal{X}^{(s+1)}). \end{cases} \quad (13)$$

Thus, we have the triangle inequality as follows,

$$\begin{aligned} \left\| \partial F(\mathcal{M}^{(s+1)}) \right\|_F & \leq \sum_{k=1}^N \sum_{i \neq k}^N \left\| \partial_{\mathbf{G}_{k,i}} f(\mathbf{G}^{(s+1)}, \mathcal{X}^{(s+1)}) \right\|_F \\ & \quad + \left\| \partial_{\mathcal{X}} f(\mathbf{G}^{(s+1)}, \mathcal{X}^{(s+1)}) \right\|_F \end{aligned} \quad (14)$$

Substitute into the first-order optimal condition (11), leading to

$$\begin{aligned} & \left\| \partial F(\mathcal{M}^{(s+1)}) \right\|_F \\ & \leq \sum_{k=1}^N \sum_{i \neq k}^N \left\| \partial_{\mathbf{G}_{k,i}} f(\mathbf{G}^{(s+1)}, \mathcal{X}^{(s+1)}) - \rho(\mathbf{G}_{k,i}^{(s+1)} - \mathbf{G}_{k,i}^{(s)}) \right\|_F \\ & \quad - \left\| \partial_{\mathbf{G}_{k,i}} f\left(\mathbf{G}_{<k,i}^{(s+1)}, \mathbf{G}_{k,i}^{(s+1)}, \mathbf{G}_{>k,i}^{(s)}, \mathcal{X}^{(s)}\right) \right\|_F \\ & \quad + \rho \left\| \mathcal{X}^{(s+1)} - \mathcal{X}^{(s)} \right\|_F \\ & \leq \sum_{k=1}^N \sum_{i \neq k}^N \left\| \partial_{\mathbf{G}_{k,i}} f(\mathbf{G}^{(s+1)}, \mathcal{X}^{(s+1)}) \right\|_F \\ & \quad - \left\| \partial_{\mathbf{G}_{k,i}} f\left(\mathbf{G}_{<k,i}^{(s+1)}, \mathbf{G}_{k,i}^{(s+1)}, \mathbf{G}_{>k,i}^{(s)}, \mathcal{X}^{(s)}\right) \right\|_F \\ & \quad + \sum_{k=1}^N \sum_{i \neq k}^N \rho \left\| \mathbf{G}_{k,i}^{(s+1)} - \mathbf{G}_{k,i}^{(s)} \right\|_F + \rho \left\| \mathcal{X}^{(s+1)} - \mathcal{X}^{(s)} \right\|_F. \end{aligned} \quad (15)$$

Since $f \in C^1$ and $h \equiv 0$, the partial derivatives $\{\partial_{\mathbf{G}_{k,i}} F(\mathcal{M})\}$ is $\{L_{k,i}\}_{k \in [N], i \in [N] \setminus k}$ -Lipschitz continuous. Then, we easily have

$$\begin{aligned} & \left\| \partial_{\mathbf{G}_{k,i}} f(\mathbf{G}^{(s+1)}, \mathcal{X}^{(s+1)}) \right\|_F \\ & - \left\| \partial_{\mathbf{G}_{k,i}} f\left(\mathbf{G}_{<k,i}^{(s+1)}, \mathbf{G}_{k,i}^{(s+1)}, \mathbf{G}_{>k,i}^{(s)}, \mathcal{X}^{(s)}\right) \right\|_F \\ & \leq L_{k,i} \left\| \left\{ \mathbf{G}_{>k,i}^{(s+1)} - \mathbf{G}_{>k,i}^{(s)} \right\}, \mathcal{X}^{(s+1)} - \mathcal{X}^{(s)} \right\|_F, \end{aligned} \quad (16)$$

Table 1. Results of PSNR, SSIM, and runtime for *toy* under different fiber missing ratios (FR). The best results are highlighted in **bold**; the second-best are underlined.

Dataset	method	80%			70%			60%			50%		
		PSNR	SSIM	time									
<i>toy</i>	Observed	11.810	0.352	—	12.351	0.417	—	13.049	0.477	—	13.836	0.533	—
	HaLRTC	13.335	0.519	20.900	14.535	0.586	25.527	16.146	0.650	23.060	17.938	0.720	24.346
	TNN	13.211	0.514	250.817	14.349	0.580	279.316	15.869	0.642	278.906	17.505	0.710	285.015
	TMac	13.401	0.441	2.184	15.775	0.536	2.851	19.326	0.646	2.864	23.441	0.730	3.120
	TFTC	<u>22.856</u>	<u>0.643</u>	57.503	23.654	0.690	29.700	24.420	0.726	23.464	25.286	0.759	12.963
	SNN	13.403	0.520	257.582	14.626	0.588	282.532	16.272	0.654	271.567	18.104	0.725	276.069
	Tucker	21.330	0.626	29.573	<u>24.408</u>	<u>0.710</u>	20.121	25.277	0.750	6.725	26.102	0.772	6.892
	TT	19.757	0.598	81.792	24.533	0.716	15.427	25.486	0.756	10.109	26.322	0.788	11.200
	FCTN	16.116	0.472	27.100	22.947	0.700	30.593	<u>27.481</u>	<u>0.779</u>	15.470	<u>28.512</u>	<u>0.816</u>	22.853
	Ours	23.141	0.656	61.384	25.186	0.730	35.671	27.615	0.802	43.864	29.320	0.846	23.363

*Although the computational complexity of iFCTN is much lower than FCTN, the closed-form update in (11) relies on extensive ‘for’ loops (over k , i , and j), which are inefficient in MATLAB, leading to longer actual CPU time.

Thus, a backsubstitution yields

$$\begin{aligned}
 & \left\| \partial F(\mathcal{M}^{(s+1)}) \right\|_F \\
 & \leq \sum_{k=1}^N \sum_{i \neq k}^N L_{k,i} \left\| \left\{ \mathbf{G}_{>k,i}^{(s+1)} - \mathbf{G}_{>k,i}^{(s)} \right\}, \mathcal{X}^{(s+1)} - \mathcal{X}^{(s)} \right\|_F \\
 & + \sum_{k=1}^N \sum_{i \neq k}^N \rho \left\| \mathbf{G}_{k,i}^{(s+1)} - \mathbf{G}_{k,i}^{(s)} \right\|_F + \rho \left\| \mathcal{X}^{(s+1)} - \mathcal{X}^{(s)} \right\|_F \\
 & \leq \left(\sum_{k=1}^N \sum_{i \neq k}^N L_{k,i} + N(N-1) \right) \left\| \mathcal{M}^{(s+1)} - \mathcal{M}^{(s)} \right\|_F \\
 & = L_F \left\| \mathcal{M}^{(s+1)} - \mathcal{M}^{(s)} \right\|_F,
 \end{aligned} \tag{17}$$

where $L_F = N(N-1)\rho + \sum_{k=1}^N \sum_{i \neq k}^N L_{k,i}$. Therefore, there exists $\mathcal{P}^{(s+1)} \in \partial F(\mathcal{M}^{(s+1)})$ such that

$$\left\| \mathcal{P}^{(s+1)} \right\|_F \leq L_F \left\| \mathcal{M}^{(s+1)} - \mathcal{M}^{(s)} \right\|_F. \tag{18}$$

The relative error condition is proved. \square

3. Details for Experiments

3.1. Parameter Details

To minimize the influence of the numerical optimizer, the Tucker, TT, and FCTN models were also solved using the PAM scheme. The algorithm parameters were set as follows: the proximal parameter $\rho = 0.1$, maximum iteration $t_{\max} = 1000$, and stopping criteria $\epsilon = 10^{-5}$.

For HaLRTC and SNN, the weight vector α was fixed to $(\frac{1}{N}, \dots, \frac{1}{N})$. The hyperparameters for TFTC, TT, and FCTN were tuned over prescribed ranges and selected manually for best performance. All datasets were pre-normalized to $[0, 1]$. In addition to random missingness

(RM), we investigated a more realistic setting with temporally correlated, fiber-wise missingness (FM), which limits the ability to borrow information across other modes.

3.2. Result Analysis

As noted in the main text, we now provide a supplementary description of the experiment.

Table 1 complements Table 2 (main text) by presenting the fiber missing results specific to *toy*. Meanwhile, Fig. 1 presents the reconstruction results and corresponding PSNR values for *flower*, *face*, and *toy*.

As shown in Table 2 and Fig. 2, the iFCTN method demonstrates consistent superiority. A notable example at RM = 90% shows iFCTN outperforming the second-best method by substantial margins: 2.3 on *flower* and *face*, and by 1.5 on *toy*, thereby clearly affirming its effectiveness.

Table 3 provides supplementary information for Fig. 4 in the main text. For example, at FM = 50%, iFCTN surpasses the second-best method on dataset *Birmingham* by a margin of 0.032 in terms of RSE, demonstrating its efficacy.

4. Experiments for the Storage Cost

We evaluate the storage cost of several decomposition methods—Tucker, TT, FCTN, and iFCTN—on the *flower* dataset of size $256 \times 256 \times 31$. All decompositions are computed using PAM to eliminate the influence of the optimization algorithm. We have

- Tucker decomposition needs 4856 parameters (0.24% of total elements) to express the testing data (Tucker rank is (8,8,8));
- TT decomposition needs 23319 parameters (1.15% of total elements) to express the testing data (TT rank is (9,9));
- FCTN decomposition needs 8688 parameters (0.45% of total elements) to express the testing data (FCTN rank is



Figure 1. The pseudo-color renderings of reconstructions (composed of the 29th, 19th, and 9th bands) and corresponding PSNRs for MSI datasets. The top, middle, and bottom rows display the *flower*, *face*, and *toy* with FM = 60%, respectively.

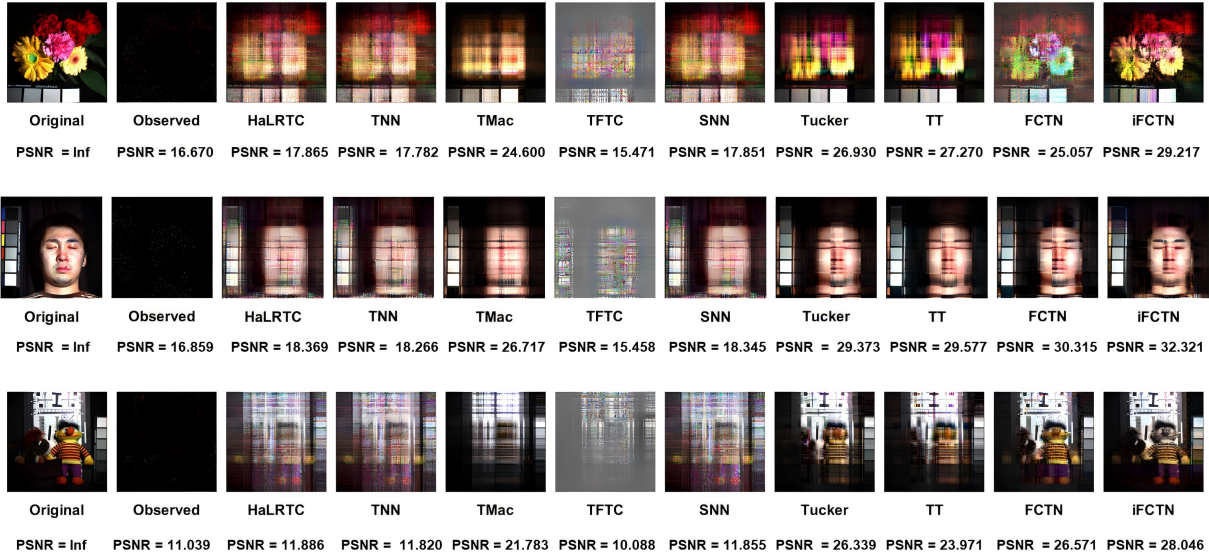


Figure 2. The pseudo-color renderings of reconstructions (composed of the 29th, 19th, and 9th bands) and corresponding PSNRs for MSI datasets. The top, middle, and bottom rows display the *flower*, *face*, and *toy* with RM = 95%, respectively.

- (4,4,4));
- iFCTN decomposition needs 4344 parameters (0.21% of total elements) to express the testing data (iFCTN rank is (0,4,4; 0,0,4; 0,0,0)) ;

These experimental results provide empirical evidence supporting the analysis regarding the superiority of the iFCTN decomposition over other decompositions in terms

of storage cost.

5. MATLAB Code

The code is available in supplement materials `iFCTN_code.zip`.

Table 2. Results of PSNR, SSIM, and runtime for *flower*, *face*, and *toy* under different random missing ratios (SR). The best results are highlighted in **bold**; the second-best are underlined.

Dataset	method	99%			95%			90%			80%		
		PSNR	SSIM	time									
<i>flowers</i>	Observed	16.489	0.365	—	16.670	0.410	—	16.906	0.423	—	17.409	0.482	—
	HaLRTC	16.586	0.412	17.979	17.865	0.612	22.242	19.355	0.680	23.421	22.380	0.766	23.046
	TNN	16.589	0.414	267.396	17.782	0.610	259.661	19.147	0.676	260.827	21.889	0.759	252.640
	TMac	17.092	0.456	1.500	26.044	0.644	1.739	25.732	0.734	3.046	26.949	0.730	1.297
	TFTC	15.400	0.283	111.247	15.471	0.440	113.304	16.886	0.506	116.664	20.437	0.578	123.250
	SNN	16.628	0.434	265.601	17.851	0.615	275.705	19.191	0.676	287.894	21.853	0.756	269.143
	Tucker	<u>21.255</u>	<u>0.482</u>	23.874	26.930	0.653	12.129	27.274	0.672	6.034	27.823	0.703	2.396
	TT	20.658	0.447	77.905	<u>27.270</u>	<u>0.659</u>	26.313	27.686	0.692	27.692	32.893	0.718	0.175
	FCTN	20.764	0.426	25.505	25.057	0.574	62.160	<u>28.690</u>	<u>0.684</u>	76.230	33.562	<u>0.790</u>	123.561
	Ours	22.152	0.486	64.516	29.217	0.758	86.854	30.996	0.832	96.751	<u>32.438</u>	0.875	98.728
<i>face</i>	Observed	16.680	0.272	—	16.859	0.305	—	17.092	0.342	—	17.601	0.410	—
	HaLRTC	16.803	0.339	19.185	18.369	0.642	22.165	20.181	0.724	23.234	24.034	0.812	23.832
	TNN	16.809	0.344	260.098	18.266	0.644	245.207	19.909	0.716	259.362	23.330	0.798	258.636
	TMac	16.630	0.270	1.502	26.717	0.757	1.580	28.603	0.798	1.973	30.231	0.846	2.203
	TFTC	16.368	0.312	108.594	15.458	0.458	112.138	18.027	0.556	111.967	19.321	0.593	112.229
	SNN	16.863	0.377	257.057	18.345	0.652	252.935	19.958	0.717	274.327	23.304	0.796	267.499
	Tucker	24.577	0.645	21.913	29.373	0.783	10.693	29.647	0.793	4.598	30.175	0.814	2.276
	TT	24.462	0.607	73.919	29.577	0.780	30.680	30.028	0.803	19.321	30.594	0.812	6.191
	FCTN	<u>26.322</u>	<u>0.659</u>	17.484	<u>30.315</u>	<u>0.816</u>	16.871	<u>30.628</u>	<u>0.823</u>	21.492	31.018	<u>0.818</u>	15.320
	Ours	27.726	0.673	56.019	32.321	0.866	56.396	32.990	0.883	50.202	33.699	0.897	52.173
<i>toy</i>	Observed	10.860	0.216	—	11.039	0.247	—	11.271	0.284	—	11.781	0.353	—
	HaLRTC	10.960	0.296	19.285	11.886	0.538	24.400	12.874	0.604	25.620	14.781	0.679	22.718
	TNN	10.961	0.301	256.624	11.902	0.538	260.471	12.733	0.604	256.402	14.487	0.672	252.102
	TMac	13.240	0.422	1.476	21.764	0.644	1.600	23.123	0.682	1.850	24.780	0.749	2.543
	TFTC	10.690	0.275	106.656	10.088	0.408	120.843	12.258	0.467	114.210	15.512	0.548	126.911
	SNN	10.987	0.326	342.048	11.855	0.546	251.225	12.752	0.602	258.321	14.669	0.672	261.822
	Tucker	<u>16.826</u>	<u>0.454</u>	29.256	23.409	0.732	26.743	26.794	0.751	12.941	27.388	0.776	6.892
	TT	15.123	0.431	75.545	23.971	0.669	77.183	24.917	0.710	75.543	25.617	0.742	50.858
	FCTN	15.211	0.424	22.774	<u>26.571</u>	<u>0.756</u>	38.070	<u>29.798</u>	<u>0.873</u>	46.431	<u>31.282</u>	0.916	81.460
	Ours	18.865	0.484	61.118	28.046	0.821	114.437	31.298	0.883	129.371	32.552	<u>0.901</u>	65.749

*Although the computational complexity of iFCTN is much lower than FCTN, the closed-form update in (11) relies on extensive ‘for’ loops (over k , i , and j), which are inefficient in MATLAB, leading to longer actual CPU time.

References

- [1] Attouch, H., Bolte, J., and Svaiter, B. F. Convergence of descent methods for semi-algebraic and tame problems: proximal algorithms, forward-backward splitting, and regularized Gauss-Seidel methods. *Math. Program.*, 137(1):91–129, 2013.
- [2] J. Bolte, S. Sabach, and M. Teboulle. Proximal alternating linearized minimization for nonconvex and non-smooth problems. *Math. Program.*, 146(1):459–494, 2014.

Table 3. Performance on RSE, RMSE, and CPU time for *Guangzhou* and *Birmingham* under different fiber missing ratios. The best results are highlighted in **bold**; the second-best are underlined.

Dataset	method	80%			70%			60%			50%		
		RSE	RMSE	time	RSE	RMSE	time	RSE	RMSE	time	RSE	RMSE	time
Guangzhou	Observed	0.894	0.337	—	0.835	0.336	—	0.775	0.336	—	0.709	0.336	—
	HaLRTC	0.566	0.213	15.979	0.388	0.156	16.277	0.242	0.105	16.430	0.131	0.062	12.126
	TNN	0.472	0.178	192.071	0.270	0.108	189.336	0.141	0.061	12.828	0.128	0.061	10.846
	TMac	0.546	0.206	2.233	<u>0.277</u>	0.111	2.331	0.165	0.071	3.136	<u>0.124</u>	<u>0.059</u>	2.937
	TFTC	0.395	0.149	44.221	0.273	0.110	42.600	0.216	0.094	40.508	0.189	0.089	42.404
	SNN	0.639	0.240	201.089	0.486	0.195	200.180	0.351	0.152	201.360	0.223	0.106	201.545
	Tucker	0.169	0.064	26.674	0.141	0.057	2.549	0.135	0.058	1.671	0.128	0.061	1.555
	TT	0.223	0.084	60.426	<u>0.141</u>	<u>0.057</u>	6.259	0.134	0.058	3.979	0.128	0.060	3.409
	FCTN	0.168	0.063	19.052	0.161	0.061	31.112	<u>0.131</u>	<u>0.057</u>	28.911	0.128	0.061	33.550
Ours	<u>0.173</u>	<u>0.065</u>	70.291	0.139	0.056	82.704	0.130	0.056	78.003	0.123	0.058	55.499	
Birmingham	Observed	0.909	0.196	—	0.807	0.184	—	0.778	0.188	—	0.700	0.181	—
	HaLRTC	0.699	0.151	0.494	0.466	0.106	0.494	0.412	0.100	0.494	0.295	0.076	0.493
	TNN	0.707	0.153	4.501	0.479	0.109	4.917	0.426	0.103	4.912	0.309	0.051	4.775
	TMac	0.801	0.173	0.053	0.544	0.124	0.060	0.491	0.119	0.063	0.323	0.066	0.072
	TFTC	0.685	0.148	1.696	0.516	0.118	1.710	0.406	0.098	1.797	0.276	0.059	1.747
	SNN	0.802	0.173	4.970	0.637	0.145	4.866	0.587	0.142	4.748	0.477	0.046	4.682
	Tucker	0.700	0.151	1.023	0.471	0.108	1.034	<u>0.210</u>	<u>0.051</u>	1.114	0.190	0.054	1.144
	TT	0.721	0.156	1.566	0.458	0.105	1.594	0.257	0.062	1.634	<u>0.210</u>	<u>0.053</u>	1.646
	FCTN	<u>0.630</u>	<u>0.136</u>	1.004	<u>0.243</u>	<u>0.056</u>	1.010	0.221	0.053	0.993	0.214	0.055	1.047
Ours	0.605	0.130	2.533	0.227	0.052	2.570	0.204	0.049	2.114	0.178	0.046	0.505	

*Although the computational complexity of iFCTN is much lower than FCTN, the closed-form update in (11) relies on extensive ‘for’ loops (over k , i , and j), which are inefficient in MATLAB, leading to longer actual CPU time.